https://doi.org/10.5194/egusphere-2024-4111
Preprint. Discussion started: 22 January 2025

A physical model for mean river discharge calculation: from riverside seismic monitoring experiments in a low-flow river, China

Xiaoyue Zhou [1], Liang Feng [1,2], Shizhe Zhang [3], Bin Xie [4], Yanmei Wang [1], Wei Xu [1], Emanuele Intrieri[5]

1. Faculty of Resource and Environmental Engineering, Jiangxi University of Science and Technology, Ganzhou, China
2. Jiangxi Provincial Key Laboratory of Water Ecological Conservation in Headwater Regions, Ganzhou, China
3. Institute of Mountain Hazard and Environment, Chinese Academy of Sciences, Chengdu, China
4. Ganzhou Earthquake Monitoring Center Station，Jiangxi Provincial Seismological Bureau, Ganzhou, China
5. Department of Earth Science, University of Florence, Florence, Italy

Correspondence to: Feng Liang（liang.feng@jxust.edu.cn）

Abstract.

The dynamics of water flow and sediment transport in river systems play a crucial role in shaping river morphology, in the planning and use of river infrastructure and the broader watershed management. However, these characteristics are often challenging to measure comprehensively. On March 17, 2023, we studied a low-flow river system (≤0.611 m³/s) within the boundaries of Yuancun in the Township of Meishui. By synchronously monitoring the microseismic signals generated by the river and the river flow velocity, we explored the relationship between these microseismic signals and the river discharge. During each experiment, we used 3 to 4 three-component seismometers placed in close proximity to the riverbank (at the distance of approximately 1 meter), with one device submerged underwater to record the microseismic signals caused by the flow. The signals exhibited a wide frequency range (2–50 Hz). An analysis of the recorded microseismic signals and the flow data revealed an approximate linear relationship between the seismic noise in the 2–10 Hz bandwidth and the river flow. We used a least squares regression model to invert the river flow from the 2–10 Hz microseismic signals and found that the maximum relative error between the inverted flow and the measured values was 10.3%. The results show that even at low flow rates, real-time monitoring of river processes is possible through continuous time-frequency analysis of microseismic signals; this increases the potential for future applications of seismic monitoring in real-time observation of hydrological evolution in river systems.

https://doi.org/10.5194/egusphere-2024-4111
Preprint. Discussion started: 22 January 2025

1 Introduction

The components of river monitoring usually include encompass river water level, flow velocity, discharge, and sediment flux. Currently, there are two main approaches to river monitoring: one is the hydrological monitoring system based on hydrological stations, and the other is the remote sensing monitoring method, which has gradually developed with the maturity of remote sensing technology. Both methods require the establishment of hydrological stations and the installation of measuring instruments, which makes the monitoring process complex, time-consuming, and resource-intensive (Roth et al.,2016; Cook et al.,2022; Larose et al.,2015). There is also a risk of the instruments being damaged and data being lost during floods. In recent years, an increasing number of researchers have explored the correlation between microseismic signal fluctuations and changes in river discharge and sediment flux, demonstrating the potential of microseismic monitoring technology for hydrological studies (Turowski et al., 2011). Since the early 1990s, when Govi et al. (1993) first deployed short-period seismometers in river channels to record microseismic signals and investigate the relationship between these signals, river discharge, and sediment transport, more researchers have begun to investigate the relationship between microseismic signals and river hydrodynamics (Rickenmann et al., 2012). Schmandt et al. (2013) have found that the sources of the microseismic signals could be related to water flow noise caused by turbulence, sediments impinging on the riverbed, or acoustic waves generated by interactions between water and the atmosphere. Díaz et al. (2014) conducted 36 months of continuous microseismic monitoring of the Aragon River and identified three types of river-induced seismic events, each with distinct characteristics related to floods caused by moderate rainfall, seasonal snowmelt, and severe storms. This demonstrates that microseismic monitoring can not only aid in studying the hydrological characteristics of rivers but also has significant potential in assessing hydrological hazards. Therefore, continuous microseismic monitoring of ambient noise generated by rivers can provide valuable insights into the study of the hydrological characteristics of rivers.

Microseismic monitoring of rivers can provide a wealth of seismic data on the vibrations of river sediments, and the interpretation of microseismic signals to infer hydrological parameters is one of the essential tasks of microseismic monitoring in rivers. Roth et al. (2016) used broadband (5–480 Hz) microseismic data, river discharge data, precipitation data, and bedload data from the Erlenbach River in the Swiss Pre-Alps to propose a simple, empirically adjusted linear model for estimating bedload transport rates. Their predictions showed a strong correlation with the transport rates determined by calibrated seismic detectors in the river. Burtin et al. (2011) analyzed a braided river with a discharge range of 1–5 m^3/s at low water levels by simultaneously measuring river discharge, bedload, and seismic signals during a limited summer period. Their analysis revealed that seismic signals in the 1–10 Hz band were most indicative of changes in the river water level, with seismic waves originating from turbulence. This demonstrates that microseismic monitoring can be used to investigate hydrological characteristics even at low discharge and can provide earlier indications of flow changes in the downstream main stem of the river (Anthony et al., 2018; Gaeuman et al.,2014).

Microseismic monitoring has practical applications in flood monitoring and early warning systems and could also be used in the future to monitor geological disasters through seismic networks. Analysis and prediction of geological hazards based on microseismic monitoring offers a significant advantage over current methods based on hydrological monitoring stations and remote sensing. By analyzing the time-frequency characteristics of microseismic signals, floods can be identified and their evolution monitored. Additionally, through inversion methods, hydrological data such as river discharge and sediment content can be derived. Microseismic technology offers a new method for online monitoring of river dynamics and flood early warning, which has enormous potential for the assessment of hydrological hazards.

This study focuses on the monitoring of tributaries with low discharge. The Jiuqu River in Yuan Village, Meishui Township, Shangyu County serves as the research object, and through experimental field studies, a microseismic monitoring system is deployed along the riverbank of the tributary to monitor the ground vibrations caused by changes in the flow to stimulate the low-frequency microseismic signals, elaborate and interpret the river microseismic signals by removing the noise of human activities, such as vehicles, from the ambient noise, analyse the physical characteristics of the river microseismic signals, and construct a mathematical model using microseismic signals to invert river flow, predicting real-time river flow (Viparelli et al.,2011), and providing a reference for monitoring and early warning of river flooding and downstream river flow changes in the region.

https://doi.org/10.5194/egusphere-2024-4111
Preprint. Discussion started: 22 January 2025

2 Experiments

2.1 Experiment sites

The river studied in this study, the Jiuqu River, is a tributary of Meishui River, located in the territory of Meishui Township in Shangyou County, China (Figure 1). Meishui Township is situated in a hilly and mountainous area with an altitude of 200-300 m, and its relative height is 50-100 m. The exposed strata are the Devonian and Carboniferous of the Late Paleozoic, and the lithology mainly consists of quartz conglomerate, quartz sandstone, siltstone and dolomitic greywacke. It slopes from north to south, with a gentle terrain, and belongs to the subtropical monsoon climate zone, with an average annual precipitation of 1,235.6 mm. In this study, four monitoring experiments were conducted at four sections of the Jiuqu River with different discharge. Current meters and seismic stations were installed on the riverbank to measure the flow velocity and seismic ambient noise in each segment. For this experiment, we selected a curved section of the Jiuqu River, approximately 1.4 kilometers long, with a river width ranging from 3 to 9 meters and a depth of 0.1 to 0.4 meters. The overall morphology of the river channel resembles that of a drainage canal, with the riverbed consisting of gravel, fine sand, and pebbles. The gravel particle size varies; the upstream section features smaller gravel particles, while the downstream section exhibits larger gravel particles (Aderhold et al., 2015). The maximum gravel size is 50 × 36 × 20 cm, with an average size of 13 × 10 × 5 cm. Some segments of the riverbed contain silt. During the experiment, water samples were taken to measure the sediment concentration, which was found to be approximately 0.5% in the studied river section. Throughout the experimental period, the river's discharge was less than 5 m^3/s, which classifyies it as a low-flow river (Figure 2).

https://doi.org/10.5194/egusphere-2024-4111
Preprint. Discussion started: 22 January 2025

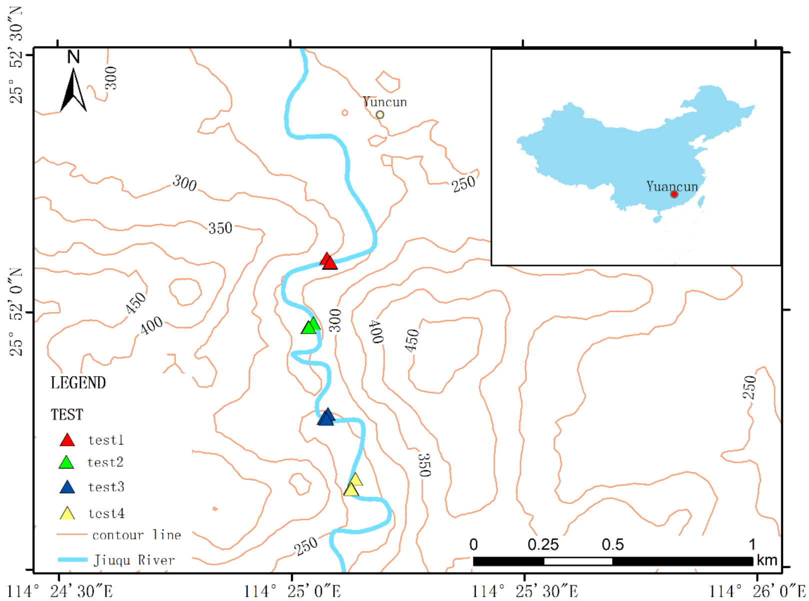

Figure 1. The geophones at the four experimental sites. The red triangles represent the three base stations in test 1, the green triangles represent the four stations in test 2, the blue triangles represent the four stations in test 3, and the yellow triangles represent the four stations in test 4.

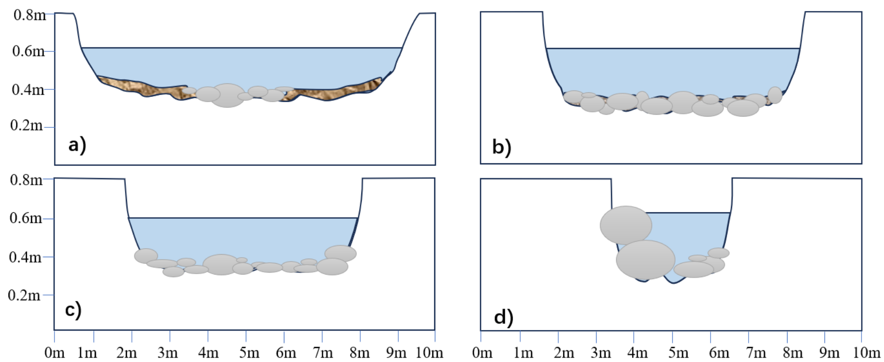

Figure 2. Cross-sectional views of the river; a), b), c), and d) are cross-sectional views of the river at the first, second, third, and fourth experimental sites, respectively. The grey ovals represent river bottom pebbles, the blue blocks represent river water, and the brown blocks represent river bottom sediment.

2.2 Seismic monitoring

Seismic ambient noise was collected from both the river sections and the nearby road areas. Seismic instruments offer a variety of sensors with different characteristics, such as accelerometer, velocimeter

https://doi.org/10.5194/egusphere-2024-4111
Preprint. Discussion started: 22 January 2025

with different Eigenfrequency and useable frequency bands, making them suitable for specific applications such as seismic imaging, monitoring, or civil engineering. The instruments can be broadly categorized into two types: short-period seismometers and geophones, which are sensitive to high-frequency bands ranging from 1 to 10 Hz up to 500 Hz. These instruments are well-suited for monitoring most geomorphological seismic sources. Surface processes also generate low-frequency seismic waves, requiring the use of broadband seismometers, which are sensitive to higher frequency signals as well. Both broadband and most short-period seismometers typically record seismic signals in three-dimensional configurations across orthogonal axes aligned vertically, north-south, and east-west, facilitating the comparison of directional information from multiple stations. The use of three-component instruments allows for greater data processing diversity compared to single-component instruments. For instance, the polarity of seismic waves can be used to determine the source type and provide information about the direction of wavefront incidence in localization problems (Burtin et al., 2014).

The seismic stations used in this experiment were four three-axis velocimeter stations (S45 triaxial velocimeter and SL06 recorder, SARA electronic instruments s.r.l., Italy), which was utilized to monitor seismic signals generated by the river, with a sensitivity factor of 78 V/m/s. The sensor components of the device were east-west (E), north-south (N), and vertical (Z). The natural frequency of these instruments was 4.5 Hz, and we set the sampling frequency for all instruments to 200 Hz. A total of four seismic stations were employed, one of which (Station 3) was an integrated velocimeters and data collector (Velbox, SARA electronic instruments s.r.l., Italy). The other three stations were separate, each equipped with a SARA 24-bit A/D converter (SL06), connected to a 24-bit digitizer via the converter. Each monitoring device was leveled using a spirit level and placed on a triangular support base to isolate it from the ground. Real-time positioning of each monitoring device was conducted using GPS, and the power supply for the monitoring devices was provided by outdoor 12 V-60 A batteries shared between different stations.

https://doi.org/10.5194/egusphere-2024-4111
Preprint. Discussion started: 22 January 2025

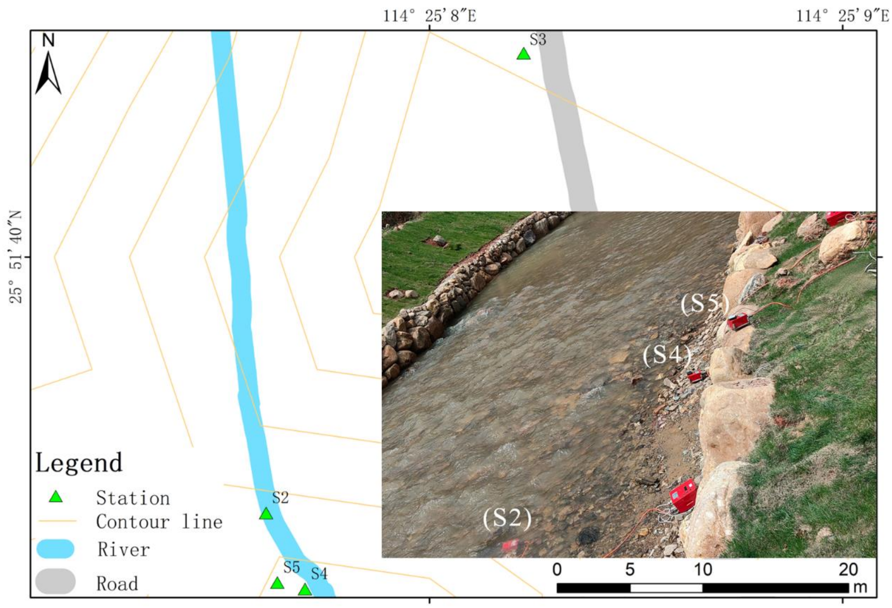

Figure 3. Detailed location distribution map of the four stations in test2, where S2 was placed in the middle of the river channel to be flooded, S4 was placed 1 m away from the river channel, S5 was placed 1.5 m away from the river channel, and S3 was placed 1.5 m from the road.

During the research period on March 17, 2024, we conducted four experiments on the Jiuqu River in Meishui Township, measuring seismic data from four river sections. Each experiment lasted for 20 minutes, during which 3 to 4 seismometers were installed approximately 1.5 meters from the riverbank to monitor the seismic signals generated by the water flow. Since the river sections are located adjacent to a road, vehicle and human activities occurred during the experiments. Therefore, in all four experiments, the S3 (Station 3) was placed about 1 meter from the riverbank, near the road. This configuration aimed to record microseismic signals generated by river activities while minimizing interference from human activities.

For the second experiment, the detailed positions of the four stations and the microseismic signals recorded by each station are illustrated in Figure 3. Given that the studied river sections are classified as low-flow segments, the instruments were placed very close to the river channel. Specifically, S2 was submerged in the middle of the river, S4 was located 1 meter from the riverbank, S5 was positioned 1.5 meters away, and S3 was situated 1.5 meters from the road (Figure 3).

https://doi.org/10.5194/egusphere-2024-4111
Preprint. Discussion started: 22 January 2025

By processing the signals recorded by the four stations and plotting the spectrograms, we found that the dominant frequency range of the microseismic signals generated by the river was between 2 and 10 Hz. In contrast, the noise frequencies generated by human activities and vehicle traffic concentrated between 7 and 25 Hz (Figure 4). Moreover, the differences in the arrangement of the stations relative to the river channel indicated that the stations were unable to monitor detailed microseismic signals at greater distances from the riverbank. This limitation is primarily due to the nature of the studied river as a low-flow system, which does not produce sufficiently strong signals.

https://doi.org/10.5194/egusphere-2024-4111
Preprint. Discussion started: 22 January 2025

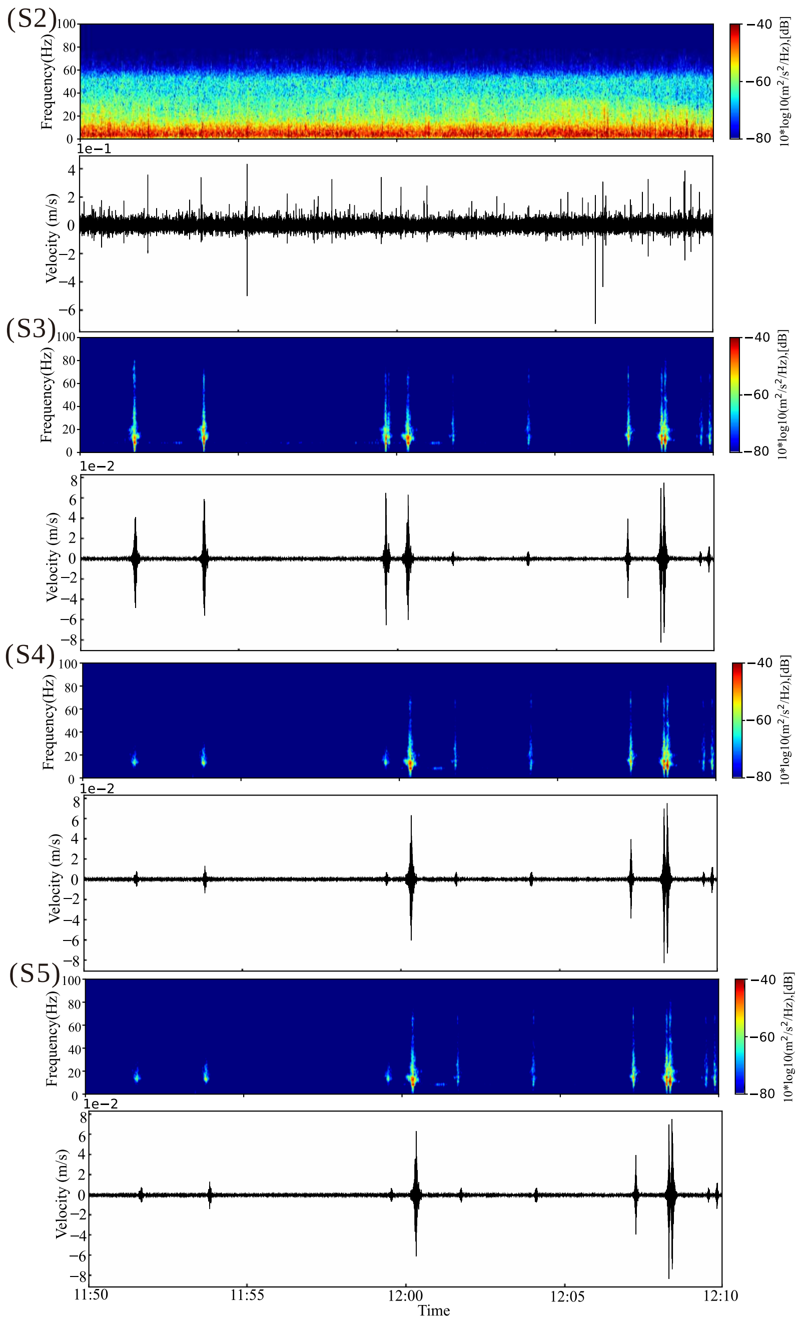

170

171 **Figure 4. Seismic waveform and spectra recorded by seismometers, S2, S3, S4, and S5, at the test 2.**

172

https://doi.org/10.5194/egusphere-2024-4111
Preprint. Discussion started: 22 January 2025

2.3 River flow velocity measurement and discharge calculation

In the study, both the flow velocity and water depth of the river sections were measured. The flow velocity was measured using a portable flow velocity meter (model LS1206B, Nanjing Jun Can Instrument Equipment Company, China). To enhance the accuracy of the measured flow velocities, vertical and horizontal sampling interval were set at 0.1 m and 1 m in a river section, respectively. In the third experiment, a continuous flow velocity meter was employed to monitor flow velocity over a period of twenty minutes.

Calculating river flow is typically achieved by determining the average flow velocity of the water passing through the measured cross-sectional area. Additionally, flow can be directly measured using appropriate devices or estimated using indirect methods such as empirical equations and mathematical models. This study utilized a common flow calculation method, the velocity-area method (Herschy, 1993). The principle of this method involves dividing the river's cross-sectional width into several slices based on the cross-section, then calculating the flow for each slice using its average slice velocity and slice area, and finally summing these to obtain the total river flow. A schematic diagram of the calculation is shown in Figure 5.

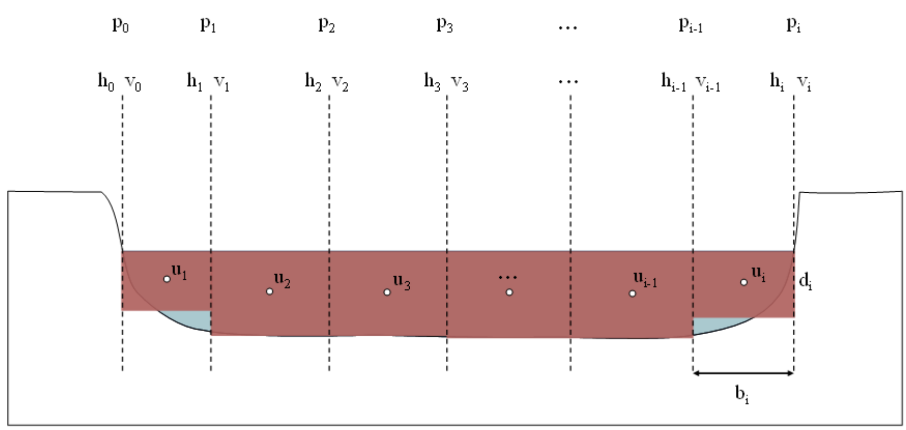

Figure 5. Schematic diagram of the velocity-area method for estimating river flows

Calculate the width of the slice b_i:

https://doi.org/10.5194/egusphere-2024-4111
Preprint. Discussion started: 22 January 2025

$$b_i = p_i p_0 - p_{i-1} p_0 \tag{1}$$

Where $p_i p_0$ denotes the distance from the *i* th vertical measurement point to the start of the riverbank.

Calculate the depth of the slice d_i

$$d_i = \frac{h_{i-1} + h_i}{2} \tag{2}$$

Where h_{i-1} and h_i are the water level measured at the *i*-1 vertical measurement point and the *i* vertical measurement point, respectively.

Multiplying the result of equation (1) with the result of equation (2) gives the slice area A_i:

$$A_i = b_i d_i \tag{3}$$

The most common methods for determining the mean slice velocity (mean vertical velocity) are the vertical velocity profile method, the two-point method and the six-tenths depth method. Since only the surface velocity of the river was measured in this experiment and that the study river is a low flow stream, the linear relationship proposed by (Genç O et al., 2015) twas used for the calculation of the mean slice velocity. The mean slice velocity u_i:

$$u_i = 0.552 \bar{u}_{wsi} \tag{4}$$

Where $\bar{u}_{wsi}$ denotes the slice-averaged water surface velocity and its value is:

$$\bar{u}_{wsi} = \frac{v_{i-1} + v_i}{2} \tag{5}$$

Where v_{i-1} and v_i are the surface flow velocity measured at the *i*-1 vertical measurement point and the *i* vertical measurement point, respectively.

The slice flow rate for each slice q_i is obtained by combining equation (3) and equation (4):

$$q_i = u_i A_i \tag{6}$$

Final river flow Q obtained: $Q = \sum_{i=1}^{n} q_i$

(7)

Where *n* denotes the number of slices.

The profile data measured in the four experiments were processed by the above calculation process to obtain the river flow rates of 0.444 m^3/s, 0.611 m^3/s, 0.512 m^3/s, and 0.598 m^3/s for tests 1, 2, 3, and 4, respectively.

https://doi.org/10.5194/egusphere-2024-4111
Preprint. Discussion started: 22 January 2025

3 Seismic ambient noise

Geophones can detect elastic waves generated by processes occurring on or near the Earth's surface, which are emitted by the transmission of energy from objects impacting the ground, such as boulders falling from slopes, pebbles bouncing on the riverbeds, or raindrops falling to the ground. The sources of elastic waves generated by river processes can be quite complex and depend on the flow configuration of the river. Possible sources include particle collisions during sediment transport, turbulence, bubble explosions, friction between water flow and riverbed or riverbanks, and the propagation of gravity waves or breaking waves on the river surface. The frequency range and physical characteristics of microseismic signals produced by different river processes are distinct. By analyzing images such as time-frequency analysis diagrams of microseismic signals, multiple overlapping seismic sources within different frequency ranges can be distinguished, and the contributions of different river processes can be extracted, thus enabling real-time monitoring of various river processes.

3.1 Human noise

Human activities can also cause seismic disturbances, such as industrial activities, vehicle noise, or people walking near seismometers. Although noise from human activity is highly variable, some typical time-frequency characteristics of noise from human activity can be highlighted. The river section studied in this research is located next to a road. During the monitoring period, vehicles driving on the road may generate signals that could affect the experiment, which is the main source of human activity during this research period. To exclude the interference from human activity, we placed the base station S3 1.5 meters away from the road in four experiments to monitor the human activities noise during the experimental period. Vehicles passing through the research section represent individual disturbances, which are of short duration and mainly affect the frequency range from 2 to 40 Hz, with high signal amplitudes and rapid attenuation of high-frequency signal amplitudes. The signal is more susceptible to attenuation with increasing distance, and is only recorded at nearby stations. As can be seen from the waveform of the microseismic signal at the S3 base station in the second experiment, the microseismic signals generated by passing vehicles are rarely coherent over the entire monitoring array (Figure 6). Therefore, the noise from human activities is not the main source of seismic energy in this study and can be largely filtered

https://doi.org/10.5194/egusphere-2024-4111
Preprint. Discussion started: 22 January 2025

out with a bandpass filter.

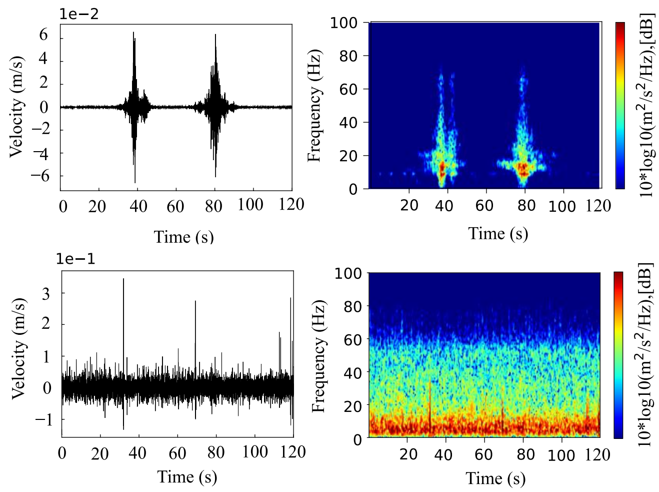

Figure 6. Waveforms and spectrograms of microseismic signals generated by the river and vehicle travelling in test2. Top: seismic signal emitted by vehicle recorded by S3 in test 2; bottom: seismic signal emitted by river recorded S2 by in test 2, 20 meters away from S3.

3.2 Still water flow

Except for the river section in the fourth experiment, which is located in a position with a steep slope and high water flow rate, the water flow in Test 1, Test 2 and Test 3, was relatively slow. Analyzing the microseismic signals and their spectral characteristics produced by the rivers in Test 1, Test 2 and Test 3, the seismic responses recorded by the monitoring stations in the three river sections share many similarities. Throughout the entire monitoring period, the seismic signals exhibit a clear broadband (2~50Hz) seismic response in both horizontal and vertical components. From the time-frequency analysis and spectral plots of Test 1 (Figure 7), the energy of the microseismic signals is distributed across the 1~50 Hz frequency band, with most of the energy concentrated in the 2~16 Hz band. In Test 2, the energy of the microseismic signals is distributed across the 1~60 Hz frequency band, with most of the energy concentrated in the 2~12 Hz band. In Test 3, the energy of the microseismic signals is distributed across the 1~50 Hz frequency band, with most of the energy concentrated in the 2~10 Hz band. By performing time-frequency analysis on the microseismic signals recorded by the monitoring stations closest to the river channel in the three experiments (namely S4, S2, and S4 stations) and calculating their Power Spectral Density (PSD), the results plotted in the same graph show that for these three experiments the

https://doi.org/10.5194/egusphere-2024-4111
Preprint. Discussion started: 22 January 2025

energy distribution is mostly concentrated in the 2~15 Hz frequency range (Figure 8).

Previous studies showed that river flow and its variations tend to excite low-frequency seismic power (1-10 Hz), that there is a significant correlation between anomalous microseismic signals in the 2-10 Hz band and river flow variations, and that the seismic power at 50 Hz has a linear relationship with the measured sediment fluxes in the riverbed (Burtin et al., 2011; Gimbert et al., 2014; Tasi et al., 2012; Díaz et al., 2014). The main frequency bands observed in this study are generally consistent with the conclusions drawn by previous scholars, and there was no significant sediment transport process during the experimental period. The seismic energy is mainly contributed by turbulence, so we can infer that the low-frequency band of 2~10 Hz in the experimental spectrum is related to the turbulent flow process of the river, and the changes in its energy reflect the changes in river flow rate.

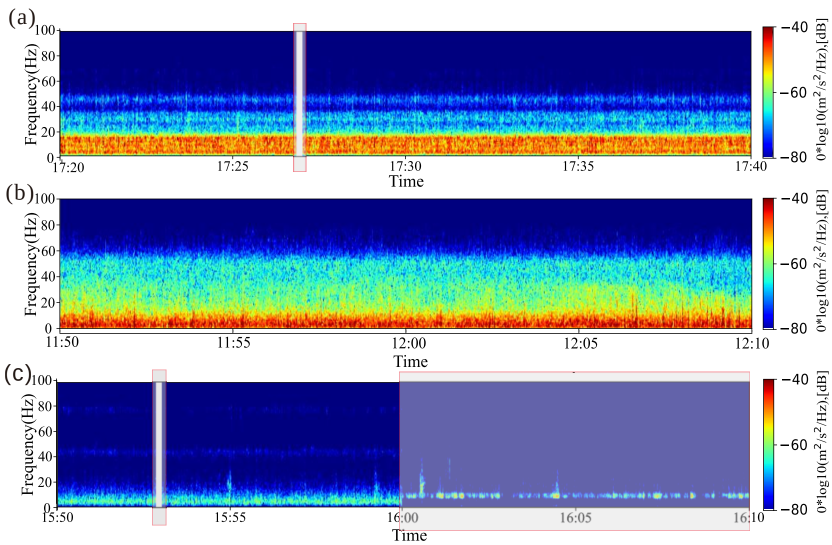

Figure 7. Spectrograms of the microseismic signals generated by the river. a), b), c) River spectrograms of the microseismic signals generated by the river at locations 1, 2 and 3 of the experiment, respectively (missing data due to instrumental interruptions are in the red boxes).

https://doi.org/10.5194/egusphere-2024-4111
Preprint. Discussion started: 22 January 2025

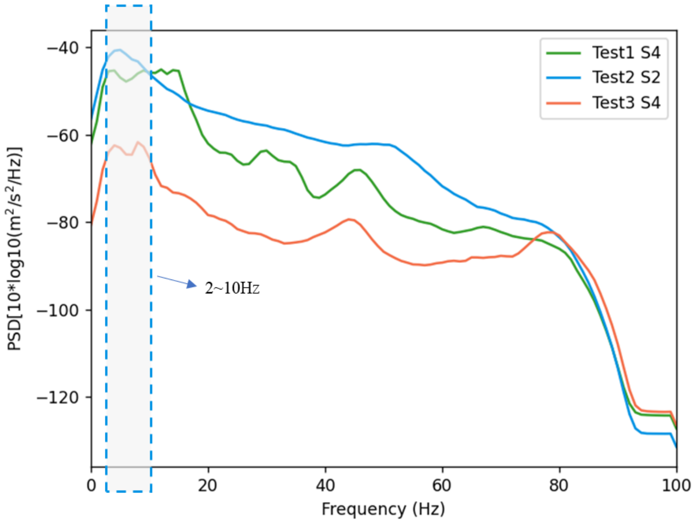

Figure 8. Acceleration power spectral density plots of microseismic signals generated by rivers. The green curve represents the PSD curve of the water flow at the nearest base station S4 of the river in test 1, the blue curve at base station S2 in test 2, the orange curve at the base station S4 in test 3; the blue dashed box highlights the frequency band of maximum energy distributions of microseismic signals of tests 1, 2, 3.

3.3 Turbulent river and sediment transport

Geophones can detect elastic waves generated by processes occurring at or near the Earth's surface. These elastic waves result from the transfer of energy produced by objects striking the ground. The sources of elastic waves generated by river processes can be quite complex, depending on the flow configuration of the river. These sources include particle collisions during sediment transport, water turbulence, bubble explosions, and the propagation of gravity waves or breaking waves on the river's surface (Figure 9). Sediment transport encompasses various particle movements, such as suspension, rolling, hopping, and sliding (Boano et al.,2011).

These river processes induce vibrations in the riverbed, generating elastic waves that propagate through the ground medium as vibrational signals. Within the range where the signal energy dissipates completely, the deployed microseismic stations can receive these signals and record them as

https://doi.org/10.5194/egusphere-2024-4111
Preprint. Discussion started: 22 January 2025

corresponding voltage fluctuations.

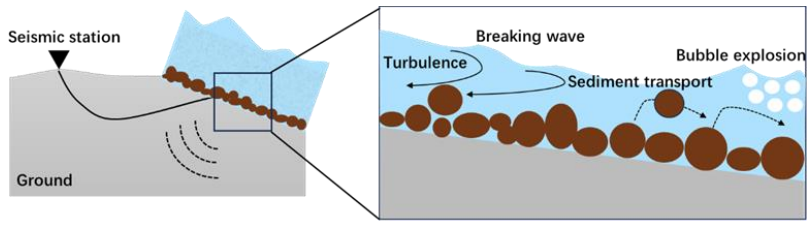

Figure 9. Seismic noise generation by turbulent flow in rivers. The brown ovals represent gravel particles in the river, which generate microseismic signals as they move with the current, the white ovals represent microseismic signals generated by the explosion of air bubbles in the water.

During the research period, the fourth experiment was conducted in a section of the river channel with large boulders that create a certain drop in the riverbed. The riverbed in this area is composed of gravel and pebbles, with the largest gravel size measured at 50×36×20 cm. The time-frequency analysis and spectral plots from this location indicate that the energy of the microseismic signals is concentrated in two distinct frequency bands, namely 2~15 Hz and 35~50 Hz, with the maximum energy located in the 7~15 Hz band (Figure 10a). The time-frequency plot from Test 2 shows that in sections of the river channel where the gradient is gentler, the energy of the microseismic signals is primarily concentrated in the 2~12 Hz frequency band (Figure 10b). Research by Burtin et al. (2011) indicates that river flow and its variations tend to excite low-frequency seismic power (1~10 Hz). Schmandt et al. (2013) found that between 35~50 Hz, this band includes frequencies (15~45 Hz) previously identified as being excited by sediment transport in river studies. Based on the data from this experimental study, it can be inferred that the seismic energy in the fourth experiment mainly originates from the river and the flow of river water driving a small amount of sediment transport to produce microseismic signals. The low-frequency band of 2~15 Hz in the spectral plot is related to the river flow process, while the higher frequency band of 35~50 Hz is associated with the river's impact on the riverbed, a small amount of sediment transport, and human activities (Barrière et al., 2015; Bagnold et al., 1966; Turowski et al., 2016). Since the river studied in this research is a low-flow river system, with no significant sediment transport phenomena observed during the experiment, a detailed exploration of the characteristics of microseismic signals generated by sediment transport was not carried out.

https://doi.org/10.5194/egusphere-2024-4111
Preprint. Discussion started: 22 January 2025

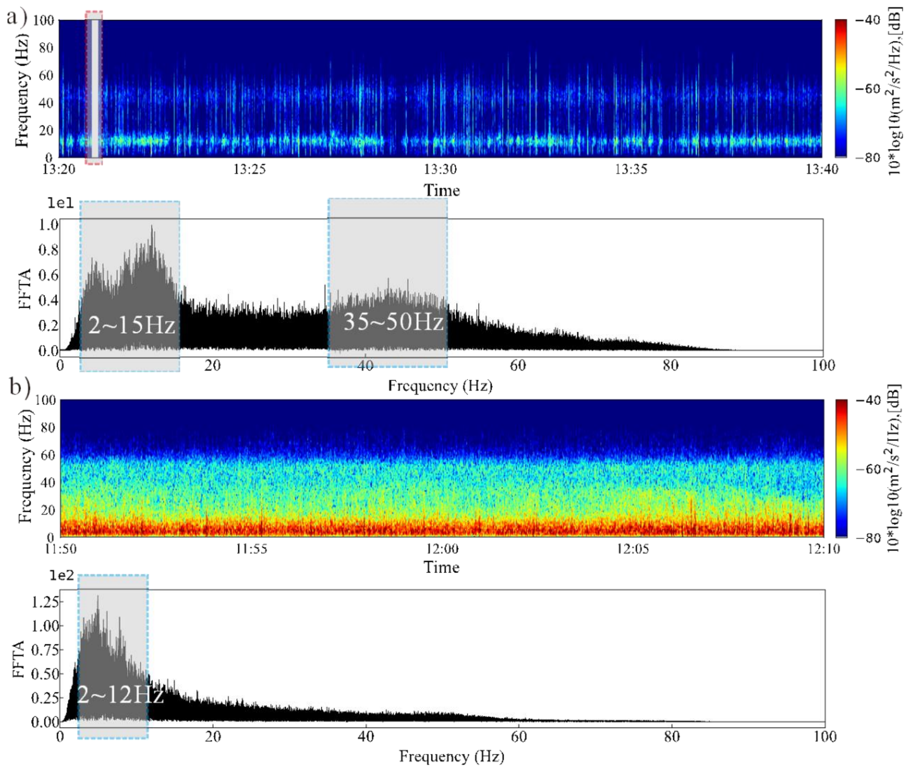

Figure 10. Time-frequency diagrams of microseismic signals generated by rivers and their spectral characteristics. a) is the time-frequency analysis and spectral characteristics of the river with a certain drop of the river section at four places of the experiment; from the time-frequency analysis, it can be seen that the energy of the microseismic signal is concentrated in the more obvious two frequency bands, respectively, 2~15 Hz, 35~50 Hz; b) is the time-frequency analysis and spectral characteristics of the river at two places of the experiment in the gently sloping section of the river, and the microseismic signal is mainly concentrated in the 2~12 Hz frequency band. The red dashed box shows missing data caused by the instrumental interruption, and the blue dashed box shows the frequency band where the energy of microseismic signals is mainly distributed.

4 Seismic interpretation and river discharge calculation

4.1 Seismic data processing

Geophones receive signals generated by rivers and record them as corresponding voltage fluctuations. These are then converted back into ground velocity based on the characteristics of the microseismic instruments, allowing for the creation of the most primitive form of seismic waveforms produced by the river signals, that is, the waveform or time series of ground velocity. The seismic amplitude of the time

https://doi.org/10.5194/egusphere-2024-4111
Preprint. Discussion started: 22 January 2025

series can provide information about the seismic signal, but some important features may be obscured by input unrelated to the monitored event. Filter processing for specific frequencies can help to filter the relevant parts of the signal. Transforming the signal to obtain the spectrum is a powerful tool for quantifying the signal amplitude in the frequency domain. It allows for rapid characterization of the signal and can be used with specific frequency filters to test and filter specific signals. However, in the spectrum, the time information is not decomposed, and the fluctuations of the spectrum in the time series are unknown. A common tool for characterizing seismic signals is time-frequency analysis, which combines both aspects, allowing the amplitude or energy of microseismic signals to be quantified in both the time domain and the frequency domain.

The Fourier transform is a classic method of time-frequency analysis. Using the Fast Fourier Transform (FFT), continuous microseismic signals are divided into short segments, and a taper is applied to the segments to obtain the spectral plot of the microseismic signal, thereby showing the distribution of seismic energy in both time and frequency. To reduce the spectral variance typically caused by the simple use of FFT and to quantify the energy produced by microseismic signals at a given frequency, we calculated the Power Spectral Density (PSD) of the time series using Welch's overlapped segment method (Welch,1967). The time series is divided into several overlapping segments, and to avoid errors when the signal is truncated, a Hamming window is used to window the segments, with a 1-second (200-sample) window having a 50% overlap, thereby obtaining a discrete 1Hz frequency band.

4.2 The relationship between river discharge and seismic noise

By discussing the source of seismic waves in the fourth section, it can be concluded that the seismic energy of the river in this study is mainly due to turbulence. The low-frequency band of 2~10 Hz in the experimental spectrum is related to the turbulent process of the river, and the changes in seismic energy reflect the changes in river flow. For verification, we selected data from the third experiment. During the third experiment, while monitoring the microseismic activity of the river, we simultaneously conducted continuous measurements of river flow velocity, measuring the average flow velocity at a distance of 1.35 m from the riverbank every minute. Based on the flow calculation formula in Section 2.3, we obtained the average flow rate per minute. The microseismic signals were selected from the S4 station,

https://doi.org/10.5194/egusphere-2024-4111
Preprint. Discussion started: 22 January 2025

which had the highest signal-to-noise ratio. Using the method of estimating the average power spectral density of the signal, we calculated the average seismic power at each frequency over a 1-minute period, and then calculated the average seismic power of the microseismic signal in the 2~10 Hz band over a 1-minute period. This was converted into energy form and plotted on the same time axis as the flow rate changes (Figure 11). It can be clearly seen from the figure that the fluctuations in the average seismic power of the three components in the 2~10 Hz band recorded by the S4 station basically match the fluctuations in the river flow at the same time, and the two have good consistency on the time scale. There are differences in the average seismic power of different components, but there are no obvious differences in the response to changes in river flow. Among them, the average seismic power change of channel N is highly consistent with the change in river flow and can well reflect the fluctuations in river flow. The above results indicate that there is a strong correlation between the recorded microseismic signals in the 2~10 Hz band and river flow. Real-time monitoring of river processes can be achieved through the analysis of the time-frequency diagram of continuous microseismic signals.

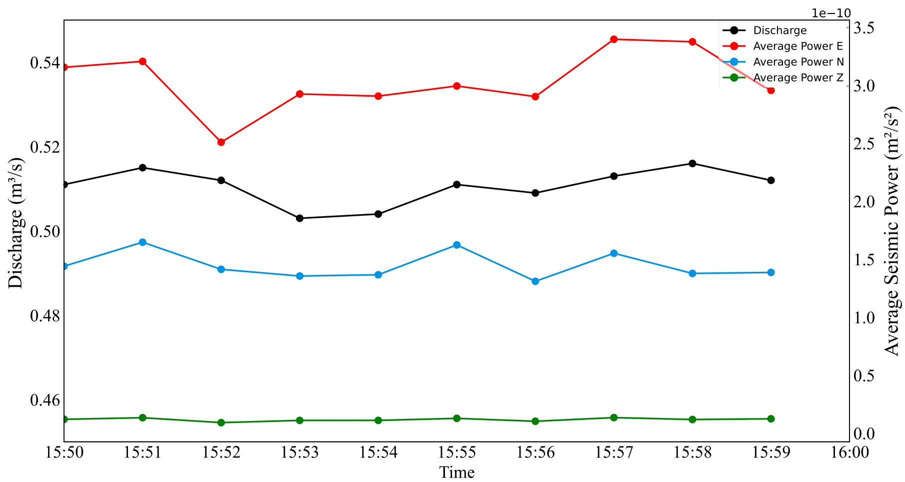

Figure 11. Mean seismic power and mean river flow correlation for Test 3. The black line represents the average flow, the red, blue and green lines represent the average seismic power of the geophone in the east-west (E), north-south (N), and vertical (Z) directions, respectively.

5 Results and discussion

This study employs a linear least squares regression model to quantify the relationship between the seismic power spectral density (PSD) above the 1 Hz band and the river turbulence, without considering the mechanical effects generated by the river process. The first 10 minutes of microseismic data from each location during the experiment were used for regression; these regressions were then used to calibrate the least squares model for flow prediction. The last 10 minutes of microseismic data from each location during the experiment were then used for testing, ultimately resulting in a linear approximation model for inferring river flow from microseismic data; the flow of the river section in the third experiment was not inverted this time, as the microseismic data for this time window experienced anomalies due to instrument issues, and could not be used for flow inversion. The total energy of the seismic waveforms generated by multiple sources is the sum of the energies in the river processes of each river section. Without considering the seismic energy generated by river sediment transport, the total seismic PSD is the sum of the PSDs produced by water turbulence (P_Q), passing vehicles (P_V), and environmental noise (P_N). When constructing the linear least squares regression model, it is assumed that the PSD generated by the first-order river turbulence process is linearly scaled with the variable representing the magnitude of that process. Therefore, for any given time t, using the seismic PSD at each frequency band (P_f), the PSD generated by road vehicles (P_{vf}), the average power of station S3 at each frequency during periods without human noise such as vehicles (P_{Nf}), and the constant linear coefficient af of flow at frequency *f*, the prediction equation for river flow $Q_{pred}(t)$ at time t is obtained:

$$Q_{pred}(t) = [P_f(t) - P_{vf}(t) - N_f]/a_f \quad (8)$$

The above equation provides the flow prediction for each frequency, which is solved using the least squares method to maximize the consistency of predictions across the 1~100 Hz. The flow regression coefficients corresponding to the highest turbulence signal-to-noise ratio geophones for each component (E, N, and Z) and each experiment site (Test 1, 2, and 4), calculated using the first 10 minutes of microseismic data, are shown in Figure 12. The regression coefficient *af* encompasses both the coupling between the flow measurement unit (m^3/s) and the ground velocity signal produced by turbulence, as well as the attenuation of each microseismic signal between the source and the geophones (the Green's function). This coefficient also represents the spectral contribution of the turbulence process to the geophones signal, or the power per frequency transmitted by unit flow.

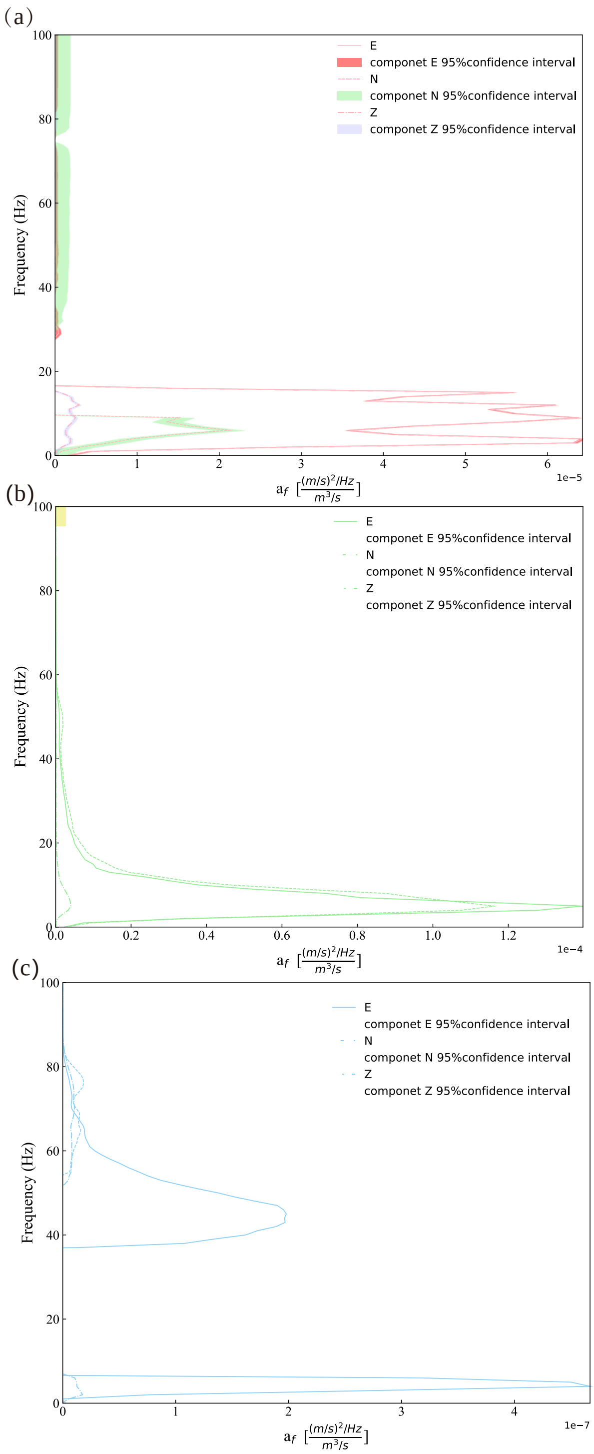

Figure 12. The flow regression coefficients and 95% confidence intervals for the river processes. (a), (b), and

https://doi.org/10.5194/egusphere-2024-4111
Preprint. Discussion started: 22 January 2025

(c) show the flow regression coefficients and 95% confidence intervals for the river processes on the E, N, and Z components of the ground motion at base stations S4, S2, and S4 at test 1, 2, and 4, respectively.

After regressing the constant linear coefficient *af* of flow at frequency *f* using the first 10 minutes of microseismic test data, the microseismic test data from the last 10 minutes is used to calculate the predicted flow values at each experimental site using the aforementioned equation. Since the flow rate calculation in this study is derived from the measured 1 minute average flow velocity, to ensure that the predicted results match the measured data, the peak values of the flow-related turbulence coefficients *af* (at frequencies of 4 Hz, 5 Hz, and 4 Hz) for the first, second, and fourth tests are substituted into the equation to calculate the river flow predicted values at every 1 minute interval during the last 10 minutes. The predicted results are compared with the flow calculation results from Section 2.3, as shown in Figure 12. From the comparison chart of the two, it can be seen that the predicted flow values established by the linear approximation model in this paper are close to the actual observed values, with the predicted flow values fluctuating around the corresponding observed values. The average values of the predicted flow values for the first, second, and fourth tests are 0.454 m^3/s, 0.548 m^3/s, and 0.537 m^3/s, respectively. The average values of the predicted flow values indicate that the results predicted by the model in this study are relatively accurate. However, the average absolute errors between the predicted flow values and the measured values for the three tests are 0.030, 0.080, and 0.237, respectively. Moreover, from Figure 13, it can be visually observed that there is a larger fluctuation between the predicted flow values and the measured values for each minute of the fourth test. This may be due to the presence of large boulders in the river section of the fourth test, which create a drop in water flow and impact the riverbed, generating noise caused by sediment transport. Additionally, during the fourth test, there were trucks and excavators operating about 150 meters away from the river section, which may have caused larger fluctuations in the predicted flow values for each minute of the fourth test. During the entire data preprocessing stage, all microseismic data were high-pass filtered to exclude the noise influence below 1 Hz, to reduce as much as possible environmental noise produced by vehicles, construction works, and other human activities,. Therefore, in this test, there is still an error between the flow prediction results obtained by inversion and the actual test results also due to the impact of the instruments' installation point, to the river flow calculation method, and the instrumental errors itself. In the future, more accurate experimental results could be obtained by starting from traditional flow refinement calculations and precise filtering

https://doi.org/10.5194/egusphere-2024-4111
Preprint. Discussion started: 22 January 2025

of river microseismic signals, increasing the number of microseismic stations, and building on the proposed model to further refine the inversion analysis.

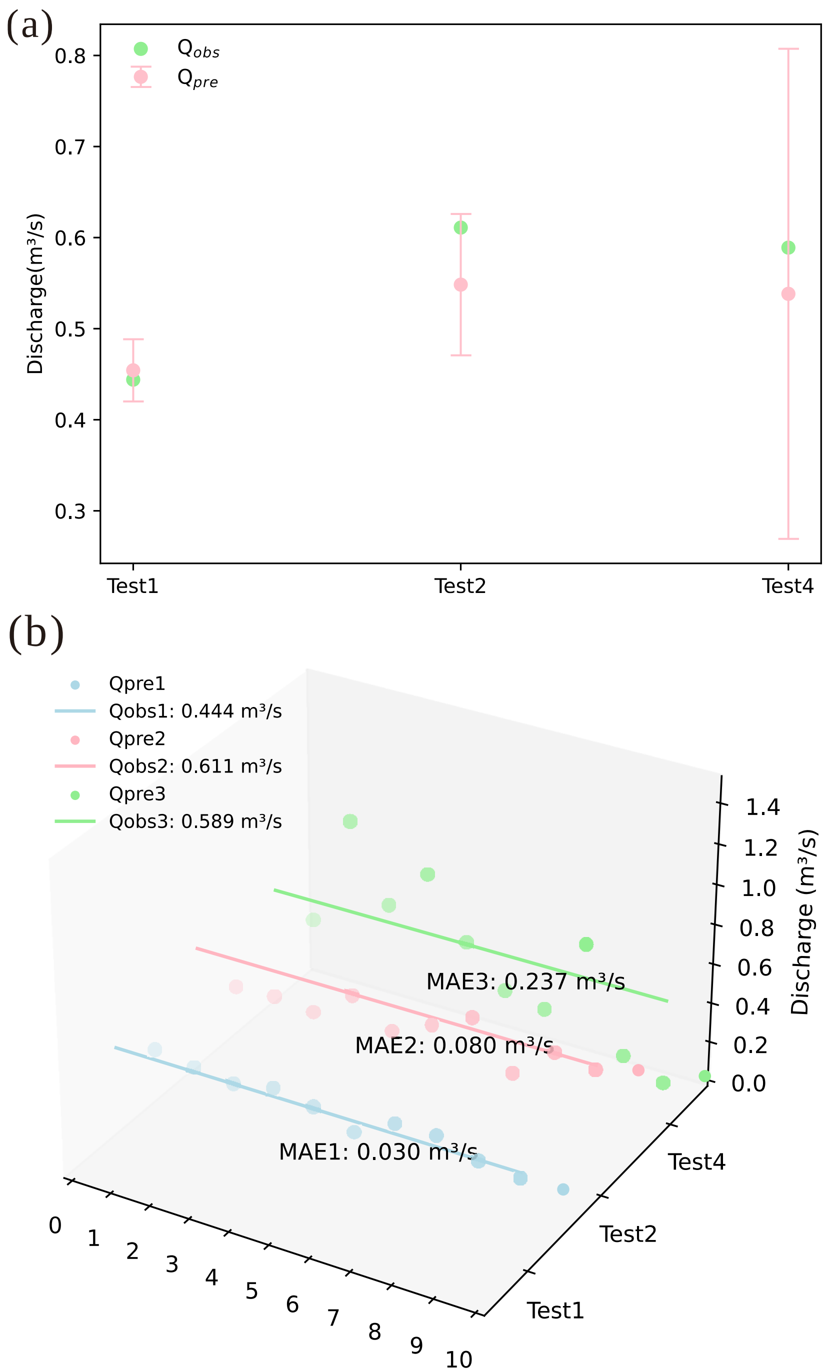

https://doi.org/10.5194/egusphere-2024-4111
Preprint. Discussion started: 22 January 2025

Figure 13. The plot of measured flow values against inverted flow predictions, (a). The scatter plot of mean absolute error between flow predictions and measured values, (b). In figure (a), green represents measured values and pink represents predicted values. In figure (b), blue represents Test1, pink represents Test2, green represents Test4, straight line represents measured flow values and scatter represents predicted values.

The linear approximation model proposed in this study for flow inversion has a relative error within 10.3%, but it also has some limitations. First, in practical situations, there is a slight nonlinear relationship between flow and seismic power, which the established model does not consider. This omission can affect the accuracy of the model inversion, leading to a reduction in inversion accuracy during practical application. Additionally, the linear approximation model proposed in this paper is built for the specific river environment in question and can be generalized to similar river environments. However, for rivers in different environments, other factors contributing to seismic power need to be considered.

6 Conclusion

The study analyzes the seismic records from 3 to 4 three-component seismometers deployed across four sections of a low-flow river system in the village and combines measurements of flow velocity and cross-sectional area of the river sections to calculate its flow data. We found that the signals generated by the river flow have a very wide frequency range (2~50Hz). Despite the presence of noise fields generated by human activities throughout the research process, which are mainly high-frequency acceleration energy, we cannot establish a correlation between high-frequency seismic power and river flow. In contrast, the recorded microseismic signals in the 2~10 Hz band have a strong connection with river flow, approximately exhibiting a linear relationship. Moreover, the microseismic signals generated by turbulence have frequencies lower than those produced by human activity noise and riverbed sediment transport and can be separated using a bandpass filter. Even with low river flow, real-time monitoring of the turbulence process can be achieved through the analysis of continuous microseismic signals time-frequency diagrams.

A linear least squares regression model was used to quantify the relationship between seismic power spectral density (PSD) above the 1 Hz band and the river turbulence process, without considering the mechanical effects generated by the river process. The first 10 minutes of microseismic data from each

https://doi.org/10.5194/egusphere-2024-4111
Preprint. Discussion started: 22 January 2025

location during the test were used for regression, and these regressions were then used to calibrate the least squares model for flow prediction. The last 10 minutes of microseismic data from each location during the experiment were then used for testing, ultimately resulting in a linear approximation model for inferring river flow from microseismic data. The predicted average values obtained from the inversion experiments for Tests 1, 2, and 4 are 0.454 m^3/s, 0.548 m^3/s, and 0.537 m^3/s, respectively, with the maximum relative error between the predicted and measured values being 10.3%. By analyzing the microseismic signals generated by vehicles and recorded at S3 in the third test and their spectral characterization, the microseismic signals in the 2~7 Hz band were retained by using a band-pass filter to minimize the impact of vehicle-related signals. The 1 minute average seismic power in the 2~7 Hz band on the time-frequency analysis map of the recorded microseismic signals was calculated by estimating the average power spectral density (Welch) of the signals and converting it into energy form; the calculated results were in good agreement with the 1 minute average flow rate measured in the field in the time scale, and showed that the time-frequency analysis based on continuous microseismic monitoring of the river can enable the monitoring of the river processes.

Author contributions. ZXY conducted the experiment, analyzed the experimental data and wrote the manuscript. ZSZ and XW participated in the experiment. WYM, XB and Emanuele Intrieri provided revision suggestions for the manuscript. FL guided the implementation of the experiment and revised the content of the manuscript.

Competing interests. The authors declare no competing interests.

References

Aderhold, K., K.E. Anderson, A.M. Reusch, M.C. Pfeifer, R.C. Aster, and T. Parker (2015), Data Quality of Collocated Portable Broadband Seismometers Using Direct Burial and Vault Emplacement, Bulletin of the Seismological Society of America, 105, 2420-2432, doi.org/10.1785/0120140352

Anthony R E, Aster R C, Ryan S, et al. (2018), Measuring mountain river discharge using seismographs emplaced within the hyporheic zone[J]. Journal of Geophysical Research: Earth Surface, 123(2): 210-228.

Burtin, A.,Bollinger, L.,Vergne, J.,Cattin, R.,&Nábělek, J.L.(2008). Spectral analysis ofseismic noiseinduced byrivers: Anewtooltomonitor spatiotemporal changes instream hydrodynamics. Journal of Geophysical Research, 113(B5),B05301. https://doi.org/10.1029/2007JB005034

https://doi.org/10.5194/egusphere-2024-4111
Preprint. Discussion started: 22 January 2025

Boano, F., R. Revelli, and L. Ridolfi (2011), Water and solute exchange through flat streambeds induced by large scale turbulent eddies, Journal of Hydrology, 403 (3), 290-296, doi:10.1016/j.hydrol.2011.03.023.

Burtin, A.,Cattin, R.,Bollinger, L.,Vergne, J.,Steer, P.,Robert, A.,etal.(2011). Towards thehydrologic andbedloadmonitoring fromhighfrequency seismic noiseinabraided river:The"torrent deStPierre", French Alps. Journal of Hydrology, 408(1–2), 43–53. https://doi.org/10. 1016/j.jhydrol.2011.07.014

Burtin, A.,Hovius, N.,McArdell, B.,Turowski, J.,&Vergne, J.(2014). Seismic constraints ondynamic links between geomorphic processes and routing ofsediment inasteep mountain catchment. Earth Surface Dynamics, 2(1),21–33. https://doi.org/10.5194/esurf-2-21-2014

Barrière, J.,Oth,A.,Hostache, R.,&Krein, A.(2015). Bedloadtransport monitoring usingseismic observations inalow-gradient ruralgravel bed stream. Geophysical Research Letters, 42(7),2294–2301. https://doi.org/10.1002/2015GL063630

Cook, K.L.,&Dietze, M.(2022). Seismic advances inprocess geomorphology. Annual Review of Earth and Planetary Sciences, 50(1),183–204. https://doi.org/10.1146/annurev-earth-032320-085133

Díaz,J.,Ruíz,M.,Crescentini, L.,Amoruso, A.,&Gallart, J.(2014). Seismic monitoring ofanAlpine mountain river. Journal of Geophysical Research: Solid Earth, 119(4),3276–3289. https://doi.org/10.1002/2014JB010955

Foulds, S., H. M. Griffiths, M. Macklin and P. A. Brewer (2014), Geomorphological records of extreme floods and their relationship to decadal-scale climate change, Geomorphology, 216: 193-207, https://doi.org/1016/j.geomorph.2014.04.003.

Govi, M.,Maraga, F.,&Moia, F.(1993). Seismic detectors forcontinuous bedloadmonitoring inagravel stream. Hydrological Sciences Journal, 38(2),123–132. https://doi.org/10.1080/02626669309492650

Gaeuman, D., 2014, High-flow gravel injection for constructing designed inchannel features: River Research and Applications, v. 30, p. 685–706, doi: 10.1002/rra.2662.

Gimbert, F., Tsai, V.C., and Lamb, M.P., 2014, A physical model for seismic noise generation by turbulent flow in rivers: Journal of Geophysical Research, v. 119, p.2209–2238, doi:10.1002/2014JF003201.

Genç O, Ardıçlıoğlu M, Ağıralioğlu N. Calculation of mean velocity and discharge using water surface velocity in small streams[J]. Flow Measurement and Instrumentation ， 2015, 41: 115-120.

Gimbert, F., Tsai, V.C., Amundson, J.M., Bartholomaus, T.C., and Walter, J.I., 2016, Subseasonal changes observed in subglacial channel pressure, size, and sediment transport: Geophysical Research Letters,

https://doi.org/10.5194/egusphere-2024-4111
Preprint. Discussion started: 22 January 2025

v. 43, p. 3786–3794, doi:10.1002/2016GL068337.

Herschy R. The velocity-area method[J]. Flow measurement and instrumentation, 1993, 4(1): 7-10.

Larose, E., Carrière, S., Voisin, C., Bottelin, P., Baillet, L., Guéguen, P., and Gimbert, F., 2015, Environmental seismology: What can we learn on earth surface processes with ambient noise?: Journal of Applied Geophysics, p. 116, v. 62–74, doi:10.1016/j.jappgeo.2015.02.001.

Rickenmann, D.,Turowski, J.M.,Fritschi, B.,Klaiber, A.,&Ludwig, A.(2012). Bedload transport measurements attheErlenbach stream with geophones andautomated basket samplers. EarthSurface Processes and Landforms, 37(9),1000–1011. https://doi.org/10.1002/esp.3225

Roth,D.L.,Brodsky, E.E.,Finnegan, N.J.,Rickenmann, D.,Turowski, J.M.,&Badoux, A.(2016). Bedload sediment transport inferred from seismic signals nearariver. J.Geophys. Res.Earth Surface, 121(4),725–747. https://doi.org/10.1002/2015JF003782

Schmandt, B.,Aster, R.C.,Scherler, D.,Tsai,V.C.,&Karlstrom, K.(2013). Multiple fluvial processes detected byriverside seismic and infrasound monitoring ofacontrolled floodintheGrand Canyon. Geophysical Research Letters, 40(18),4858–4863. https://doi.org/10.1002/ grl.50953

Turowski, J.M.,Badoux, A.,&Rickenmann, D.(2011). Startandendofbedload transport ingravel-bed streams. Geophysical Research Letters, 38(4),L04401. https://doi.org/10.1029/2010GL046558

Tsai, V. C., B. Minchew, M. P. Lamb, and J.-P. Ampuero (2012), A physical model for seismic noise generation from sediment transport in rivers, Geophys. Res. Lett., 39, L02404, doi:10.1029/2011GL050255.

Tsai, V. C., B. Minchew, M. P. Lamb, and J.-P. Ampuero (2012), A physical model for seismic noise generation from sediment transport in rivers, Geophysical Research Letters, 39, L02404, doi: 10.1029/2011GL050255.

Turowski, J.M., and Bloem, J.-P., 2016, The influence of sediment thickness on energy delivery to the bed by bedload impacts: Geodinamica Acta, v. 28, p.199–208, doi:10.1080/09853111.2015.1047195.

Viparelli, E., Gaeuman, D., Wilcock, P.R., and Parker, G., 2011, A model to predict the evolution of a gravel bed river under an imposed cyclic hydrograph and its application to the Trinity River: Water Resources Research, v. 47, W02533, doi:10.1029/2010WR009164.

Welch, P. D. (1967), The use of fast Fourier transform for the estimation of power spectra: A method based on time averaging over short, modified periodograms, IEEE Trans. Audio Electroacoust., 15(2), 70 – 73.